

Barocaloric effect in ferroelastic $Pb_3(VO_4)_2$

Pengtao Cheng(程鹏涛), Zuhua Chen(陈祖华), Chengliang Zhang(张成亮), Zhengming Zhang(张正明), Bing Li(李昺), and Dunhui Wang(王敦辉)

Citation: Chin. Phys. B, 2025, 34 (**3**): 036801. DOI: 10.1088/1674-1056/ada9d8
Journal homepage: http://cpb.iphy.ac.cn; http://iopscience.iop.org/cpb

What follows is a list of articles you may be interested in

High-energy x-ray diffraction study on phase transition asymmetry of plastic crystal neopentylglycol

Zhe Zhang(张哲), Yan-Na Chen(陈艳娜), Ji Qi(齐迹), Zhao Zhang(张召), Koji Ohara, Osami Sakata, Zhi-Dong Zhang(张志东), and Bing Li(李昺)
Chin. Phys. B, 2022, 31 (**3**): 036802. DOI: 10.1088/1674-1056/ac140c

Extended phase diagram of $La_{1-x}Ca_xMnO_3$ by interfacial engineering

Kexuan Zhang(张可璇), Lili Qu(屈莉莉), Feng Jin(金锋), Guanyin Gao(高关胤), Enda Hua(华恩达), Zixun Zhang(张子璒), Lingfei Wang(王凌飞), and Wenbin Wu(吴文彬)
Chin. Phys. B, 2021, 30 (**12**): 126802. DOI: 10.1088/1674-1056/ac003e

The influence of surface effects on Frederiks transition in nematic liquid crystal doped with ferroelectric nanoparticles

Erfan Kadivar, Mojtaba Farrokhbin
Chin. Phys. B, 2018, 27 (**4**): 046801. DOI: 10.1088/1674-1056/27/4/046801

Phase transition and critical behavior ofspin-orbital coupled spinel ZnV_2O_4

Li Wang(王理), Rong-juan Wang(王蓉娟), Yuan-yuan Zhu(朱媛媛), Zhi-hong Lu(卢志红),Rui Xiong(熊锐), Yong Liu(刘雍), Jing Shi(石兢)
Chin. Phys. B, 2016, 25 (**1**): 016802. DOI: 10.1088/1674-1056/25/1/016802

An effective-field theory study of hexagonal Ising nanowire：Thermal and magnetic properties

Yusuf Kocakaplan, Ersin Kantar
Chin. Phys. B, 2014, 23 (**4**): 046801. DOI: 10.1088/1674-1056/23/4/046801

Barocaloric effect in ferroelastic $Pb_3(VO_4)_2$

Pengtao Cheng(程鹏涛)[1,2], Zuhua Chen(陈祖华)[3,4], Chengliang Zhang(张成亮)[1], Zhengming Zhang(张正明)[1], Bing Li(李昺)[5,6], and Dunhui Wang(王敦辉)[1,†]

[1] *Hangzhou Dianzi University, Hangzhou* 310018, *China*
[2] *National Laboratory of Solid State Microstructures, Nanjing University, Nanjing* 210093, *China*
[3] *Center for Crystal Research and Development, Key Laboratory of Functional Crystals and Laser Technology, Key Laboratory of Cryogenics, Technical Institute of Physics and Chemistry, Chinese Academy of Sciences, Beijing* 100190, *China*
[4] *Center of Materials Science and Optoelectronics Engineering, University of Chinese Academy of Sciences, Beijing* 100049, *China*
[5] *Shenyang National Laboratory for Materials Science, Institute of Metal Research, Chinese Academy of Sciences, Shenyang* 110016, *China*
[6] *School of Materials Science and Engineering, University of Science and Technology of China, Hefei* 230026, *China*

(Received 8 October 2024; revised manuscript received 4 December 2024; accepted manuscript online 14 January 2025)

The barocaloric effect is considered as one of the most promising refrigeration with the potential to replace traditional gas compression refrigeration. One of the main obstacles to the application of barocaloric materials lies in the requirement for high driving pressures. In this paper, we report on the barocaloric effect of $Pb_3(VO_4)_2$, which exhibits a ferroelastic transition from a high-temperature trigonal structure to a low-temperature monoclinic structure at 357 K, accompanied by a substantial volume change. The entropy change induced by hydrostatic pressure can reach up 14 $J{\cdot}kg^{-1}{\cdot}K^{-1}$ under a relatively low pressure of 80 MPa. This work is expected to expand the selection range of barocaloric materials.

Keywords: solid-state refrigeration, barocaloric effect, ferroelastic transition

PACS: 68.35.Rh, 62.50.–p, 81.40.Vw, 07.20.Mc

DOI: 10.1088/1674-1056/ada9d8 **CSTR:** 32038.14.CPB.ada9d8

1. Introduction

Conventional vapor compression refrigeration technology is extensively employed in diverse areas including air conditioning, industrial refrigeration, and pharmaceutical storage. However, it would result in significant emissions of greenhouse gases, thereby not meeting contemporary standards for environmental preservation and energy efficiency. Consequently, solid-state refrigeration that is based on caloric effects has received substantial focus considering that the working substances are emission-free and environmentally friendly. Solid-state refrigeration refers to change of entropy and adiabatic temperature in response to external fields. Depending on the type of external fields, such as magnetic field, uniaxial stress, electrical field, and hydrostatic pressure, the caloric effect are categorized as magnetocaloric effect (MCE),[1,2] electrocaloric effect (ECE),[3,4] elastocaloric effect (eCE),[5,6] and barocaloric effect (BCE).[7,8]

The BCE refrigeration has received extensive attention over the past decade. In general, significant BCE can be frequently achieved at low pressures (such as < 100 MPa), comparable to MCE induced by substantial magnetic fields larger than 3 T, ECE by electric fields in the magnitude of $kV{\cdot}m^{-1}/MV{\cdot}m^{-1}$, or eCE by uniaxial stress larger than 500 MPa. The excessive magnetic fields require expensive and heavy rare-earth-based permanent magnets, and excessive voltage would cause electrical breakdown phenomena. By comparison, a hydrostatic pressure of less than 100 MPa is more easily accessible. Besides, the BCE performance of the materials is less affected by cycling fatigue characteristics. More important, the BCE materials do not have systematic selectivity. Any substance exhibiting volume changes under hydrostatic pressure can potentially exhibit BCE. Therefore, the BCE is considered the most promising alternative to traditional gas compression refrigeration. Until now, BCE has been observed in a diverse array of materials, including MCE materials,[9–12] hybrid organic–inorganic compounds,[13,14] ferroelectrics,[15,16] superionic conductors,[17,18] fluorides and oxyfluorides,[19–21] frustrated antiferromagnets,[22,23] plastic crystals.[24,25] These materials exhibit significant barocaloric entropy changes associated with magnetic, electrical, and structural phase transitions. However, BCE materials undergoing ferroelastic phase transitions remain rarely reported. Ferroelastic materials are characterized by spontaneous strain modulation in reaction to external mechanical stress, often accompanied by lattice structural changes and substantial volume change across a first-order ferroelastic-to-paraelastic phase transition. Such materials hold promise for achieving significant BCE performance.

One of the primary challenges in practical application of BCE materials lies in achieving substantial BCE entropy changes only at relatively high driving pressures. Applying excessive pressure in practical applications would increase

†Corresponding author. E-mail: wangdh@hdu.edu.cn

© 2025 Chinese Physical Society and IOP Publishing Ltd. All rights, including for text and data mining, AI training, and similar technologies, are reserved.

power consumption and equipment instability. Currently, the optimal driving pressure for most leading BCE materials typically exceeds 200 MPa.[11,26] Recently, the driving pressure of some newly discovered BCE materials has been reduced to 100 MPa.[27,28] Nonetheless, achieving excellent BCE performance at lower driving hydrostatic pressures remains a significant challenge. Additionally, evaluating the pressure coefficient dT_t/dP of materials, which quantifies the change in phase transition temperature induced by hydrostatic pressure, has emerged as an effective approach for assessing pressure sensitivity. This parameter is also crucial in determining the suitability of materials for efficient and low-pressure BCE applications.

In this paper, we report the BCE performance of lead orthovanadate $Pb_3(VO_4)_2$ possessing a ferroelastic phase transition. This vanadate belongs to the $Pb_3(XO_4)_2$ family of compounds (X = P, As, V).[29,30] It shows a first-order phase transition from ferroelastic to paraelastic phases at 357 K, accompanied by significant volume changes.[31] Moreover, the phase diagram of $Pb_3(XO_4)_2$ shows that the phase transition temperature decreases with increasing pressure.[32,33] It exhibits an entropy change of 14 $J{\cdot}kg^{-1}{\cdot}K^{-1}$ at the phase transition temperature under a relatively low pressure of 80 MPa. We suggest the ferroelastic phase transition oxide as a novel category of BCE materials, showing potential for BCE refrigeration applications.

2. Experimental methods

The $Pb_3(VO_4)_2$ sample was synthesized using the solid-state reaction method. V_2O_5 and PbO reagent grade chemicals were mixed in a molar ratio of 1:3 and placed in an alumina crucible. The mixture was heated at 1000 °C for 1 day, followed by grinding and further heating at 1200 °C for 2 days, then cooling to room temperature. The phase structure was analyzed by variable temperature x-ray diffraction (XRD) patterns with Cu-$K\alpha$ radiation in the temperature range of 340 K to 390 K. Variable temperature Raman spectroscopy was tested with the aid of *in situ* variable temperature test platform (HCP421V-MP) purchased from Instec Inc. and achieving large range, rapid, stable heating and cooling processes. Heat flow measurements under selected hydrostatic pressures were conducted using the DSCμDSC 7 EVO, which integrated a pneumatic system capable of applying hydrostatic pressure up to 100 MPa using high-pressure nitrogen. The scanning rate was 0.1 $K{\cdot}min^{-1}$, and the low rate of temperature ensured the accuracy of the test data. For pressure testing, the sample was enclosed in a high-pressure container, and the desired pressure was controlled by a dedicated high-pressure gas panel. The first-principles based on density functional theory (DFT) were performed calculate the formation energy and band gap using the AMS-BAND software.

3. Results and discussion

Figure 1 shows the XRD patterns of the $Pb_3(VO_4)_2$ measured at 350 K and 360 K, which can characterize the phase structure across the ferroelastic transition. All diffraction peaks are indexed based on the standard reference card. At the temperature of 360 K, $Pb_3(VO_4)_2$ exhibits a trigonal structure within the R-3m space group. Upon cooling to 350 K, a transition to a monoclinic structure characterized by the $P2_1/c$ space group is observed. This change of XRD pattern suggests that the phase transition temperature of $Pb_3(VO_4)_2$ occurs between 350 K and 360 K.

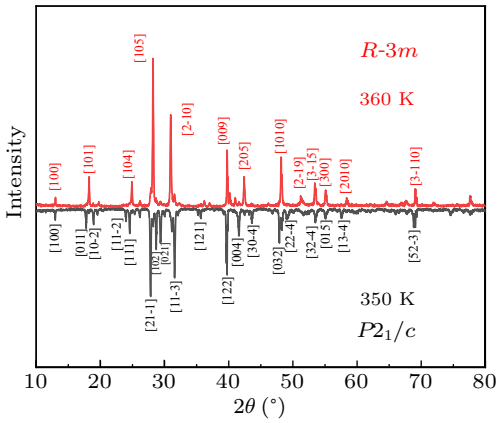


Fig. 1. The XRD patterns of the $Pb_3(VO_4)_2$ at 350 K and 360 K.

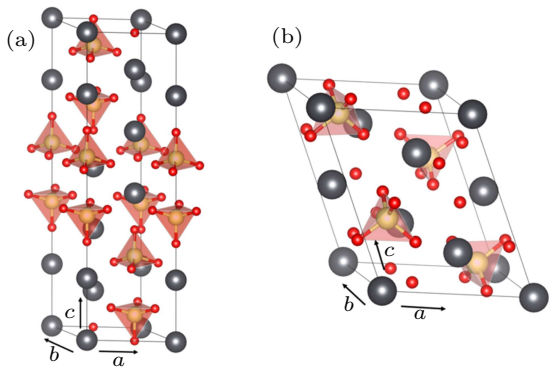


Fig. 2. Crystal structure of the $Pb_3(VO_4)_2$ sample: (a) high-temperature trigonal phase, (b) low-temperature monoclinic phase. The black sphere represents the Pb atom, the yellow sphere represents the V atom, and the red sphere represents the O atom.

Two different crystal structures of the $Pb_3(VO_4)_2$ sample are illustrated in Fig. 2. In $Pb_3(VO_4)_2$ crystals, Pb-layers and O_4-layers are stacked along the c-axis, with V atoms coordinated by four nearest neighbor O atoms to form $[VO_4]$ tetrahedra. In the case of trigonal phase at high temperature, the V atom predominantly occupies a central position within the $[VO_4]$ tetrahedra. The stacking of atomic layers is orthogonal to threefold axis. Upon cooling, $Pb_3(VO_4)_2$ undergoes a phase transition from a trigonal structure to a monoclinic structure. The V atom at the center of the $[VO_4]$ tetrahedra and Pb atom originally along the threefold axis displace, and the threefold symmetry is broken.

In order to obtain further insight into the structure of $Pb_3(VO_4)_2$, the phase transition was investigated by means of variable temperature Raman spectroscopy. As shown in Fig. 3, the Raman spectrum consists of three groups locating at 50 cm^{-1} to 240 cm^{-1}, 300 cm^{-1} to 400 cm^{-1} and 700 cm^{-1} to 900 cm^{-1} regions, respectively. In the bands lying in the 50 cm^{-1} to 240 cm^{-1} range that are attributed to external modes of the lattice, a modification of the spectra can be observed between 350 K and 360 K. The spectra at 360 K and 350 K have a typical band locating at 150 cm^{-1} and 214 cm^{-1}, respectively. This phenomenon indicates that the external lattice vibration mode of $Pb_3(VO_4)_2$ is changed. Furthermore, the band of 317 cm^{-1} that is assigned to the vibrations of $(VO_4)^{3-}$ ion shifts to 325 cm^{-1}. These changes in Raman spectra correspond to the distortion of $[VO_4]$ tetrahedra in the crystal structure across the phase transition from high-temperature trigonal phase to low-temperature monoclinic phase between 350 K and 360 K. These structural changes across the phase transition suggest that $Pb_3(VO_4)_2$ has the potential to show a significant BCE.

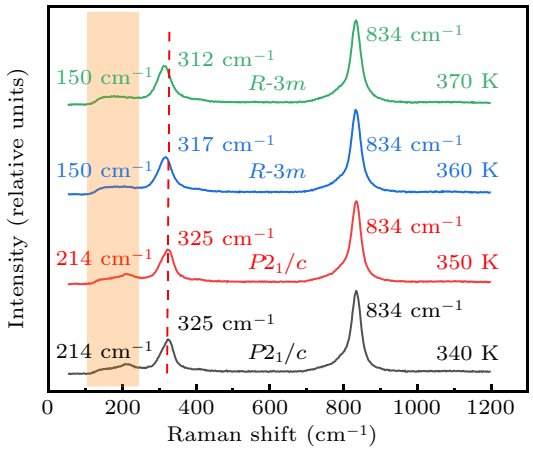


Fig. 3. Raman scattering spectra of the $Pb_3(VO_4)_2$ sample recorded between 340 K and 370 K.

Deriving barocaloric entropy changes from isobaric calorimetric curves is a commonly accepted quasi-direct method for assessing the barocaloric performance. The temperature-dependent heat flow profiles are recorded under several selected hydrostatic pressures up to 80 MPa, which is depicted in Fig. 4(a). These profiles manifest distinct peaks at transition temperatures, denoted as T_t. The T_t value for the ferroelastic phase transition at ambient pressure is determined to be 357 K, which is consistent with corresponding deductions derived from XRD analyses either. With increasing pressure, a noticeable downward shift of T_t is observed. This means the pressure tends to stabilize the trigonal phase, which has a smaller unit cell volume compared to the monoclinic phase. The rate at which the phase transition temperature moves with pressure, which is called as the pressure coefficient dT_t/dP, is calculated to be 120 K/GPa for both cooling and heating cycles, as shown in Fig. 4(b). It is worth to note that the pressure coefficient of $Pb_3(VO_4)_2$ exceeds that of most previously reported barocaloric materials to date, such as 18 K/GPa for $Ni_{49.26}Mn_{36.08}In_{14.66}$,[9] 94 K/GPa for $LaFe_{11.33}Co_{0.47}Si_{11.2}$,[10] 35 K/GPa for $Gd_5Si_2Ge_2$,[11] 50 K/GPa for $(NH_4)_2SO_4$,[15] and so forth. This indicates the extreme sensitivity of $Pb_3(VO_4)_2$ to hydrostatic pressure, suggesting its potential for generating large entropy changes even under relatively low hydrostatic pressures.

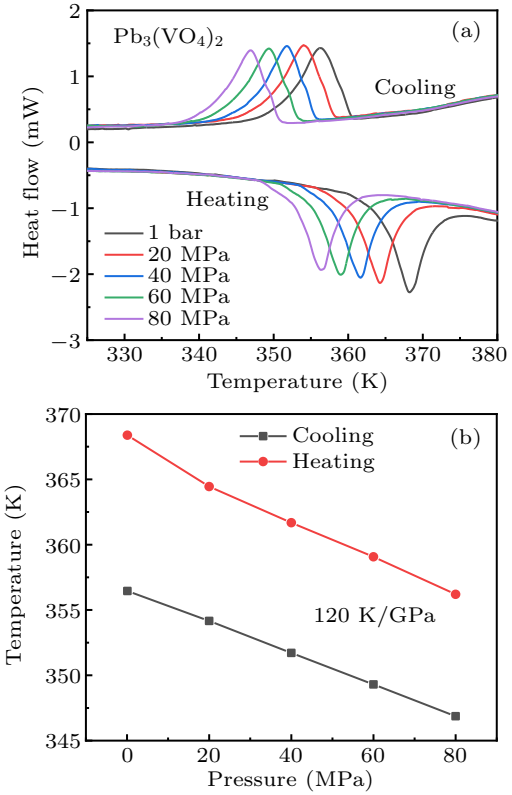


Fig. 4. (a) Heat flow data for the $Pb_3(VO_4)_2$ sample for both cooling and heating cycles under several hydrostatic pressures up to 80 MPa. (b) Transition temperatures as a function of hydrostatic pressure.

From the measured heat flow data under selected hydrostatic pressures, the isobaric entropy change across the first-order phase transition can be calculated using the following equation:

$$S(T,P) - S(T_0,P) = \int_{T_0}^{T} \frac{1}{T} \frac{\dot{Q}(P)}{\dot{T}} \mathrm{d}T, \tag{1}$$

where $\dot{Q}$, $\dot{T}$, and P represent the heat flow, rate of transition temperature change, and hydrostatic pressure, respectively. The integral is based on heat flow data with the baseline subtracted, focusing solely on the contribution from the ferroelastic transition. The calculated isobaric transition entropy observed across the ferroelastic transition for both cooling and heating runs is plotted in Figs. 5(a) and 5(b), respectively. It can be found that the isobaric transition entropy reaches up 14 $J{\cdot}kg^{-1}{\cdot}K^{-1}$. Besides, based on pressure coefficient dT_t/dP and the isobaric transition entropy, the spontaneous fractional

volume change Δv across the first-order ferroelastic transition can be estimated by the Clausius–Clapeyron relation

$$\frac{\mathrm{d}T_\mathrm{t}}{\mathrm{d}P} = V_\mathrm{m} \cdot \left(\frac{\Delta v}{\Delta S}\right)_{T=T_\mathrm{t}}, \tag{2}$$

where V_m is the molar volume. The volume change Δv at T_t is calculated to be -1.5%, which is in agreement with the results reported by Midorikawa.[32] The studies on thermal expansion indicate notable reductions in strains along distinct crystallographic directions — Δc, Δa_1 and Δa_2. This substantial volume change during the first-order ferroelastic transition plays a crucial role in contributing to the isobaric transition entropy of $Pb_3(VO_4)_2$.

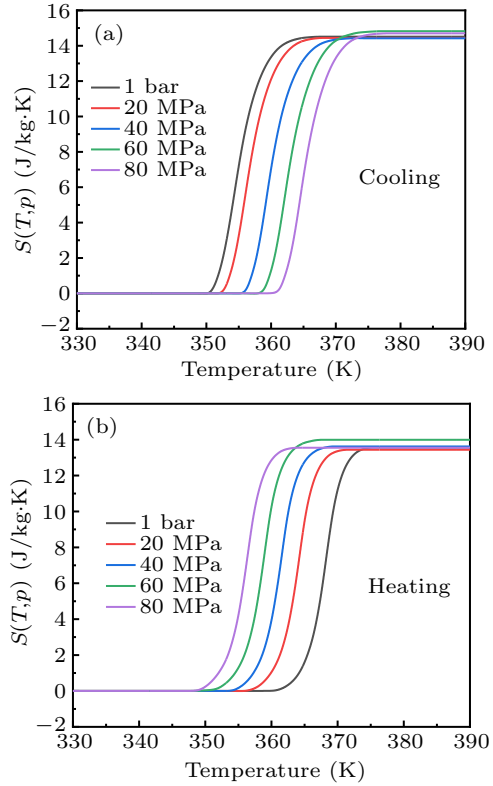


Fig. 5. Temperature dependence of isobaric transition entropy for the $Pb_3(VO_4)_2$ sample on (a) cooling and (b) heating at various pressures obtained from heat flow data.

By subtracting the isobaric transition entropy curves measured under several selected hydrostatic pressure to the one measured under ambient pressure, the pressure-induced barocaloric entropy change (ΔS_BCE) can be obtained by

$$\Delta S_\mathrm{BCE}(0 \to p) = S(T,p) - S(T,0), \tag{3}$$

$$\Delta S_\mathrm{BCE}(p \to 0) = S(T,0) - S(T,p). \tag{4}$$

The results are plotted in Figs. 6(a) and 6(b), respectively, illustrating the expected trend where ΔS_BCE increases proportionally with applied pressure. Moreover, the $Pb_3(VO_4)_2$ sample shows a maximum value of 14 $\mathrm{J{\cdot}kg^{-1}{\cdot}K^{-1}}$ achieved under the pressure of 80 MPa, which is readily accessible under conventional condition. It is noteworthy that even at 40 MPa, the entropy change retains a substantial value of up to 11 $\mathrm{J{\cdot}kg^{-1}{\cdot}K^{-1}}$. Up to now, the barocaloric materials that exhibit large entropy changes under such low pressure are rarely reported. For practical applications, excessive pressure application can lead to increased power consumption and equipment instability. The characteristic of $Pb_3(VO_4)_2$ being responsive to lower pressures holds considerable promise for practical applications.

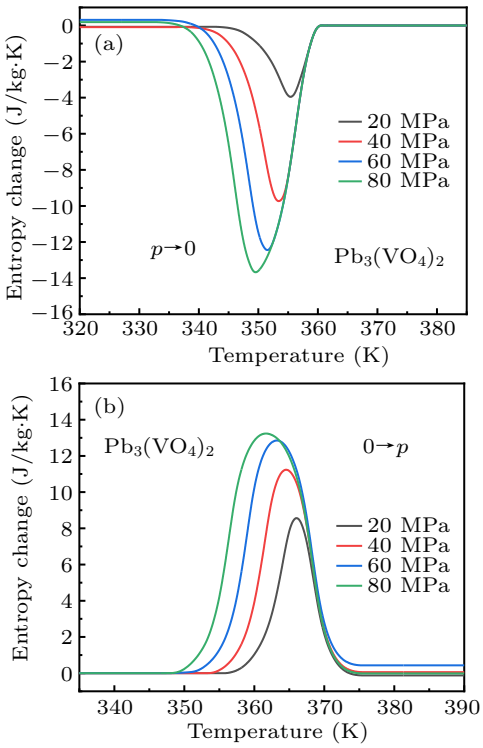


Fig. 6. Pressure-induced barocaloric entropy change as a function of temperature for (a) $p \to 0$ and (b) $0 \to p$.

Based on thermodynamic theory, the transition entropy change at finite temperature can be calculated by the Gibbs free energy formula

$$\Delta G = \Delta H - T\Delta S. \tag{5}$$

Here, ΔG and ΔH represent Gibbs free energy and enthalpy, respectively. We use first principles DFT to estimate the formation energy of $Pb_3(VO_4)_2$ between two phases. The DFT-based first principles calculations for structure were carried out with Vienna *Ab initio* Simulation Package (VASP) plane wave *ab initio* code using general gradient approximation (GGA).[34,35] Based on DFT calculation, the difference in formation energy between the high-temperature trigonal phase and the low-temperature monoclinic phase, also known as enthalpy change, is 1.307 kcal/mol. By substituting ΔH between the two phases into the formula, the entropy change value of $Pb_3(VO_4)_2$ at 357 K is calculated to be 17.9 $\mathrm{J{\cdot}kg^{-1}{\cdot}K^{-1}}$, which is similar to the experimental result.

It is well known that the total entropy change is the sum of the changes of magnetic entropy, electronic entropy, and lattice entropy. Based on DFT calculation, the band gap of

high-temperature trigonal phase and low-temperature monoclinic phase is calculated to be 2.84 eV and 2.79 eV, respectively, indicating that $Pb_3(VO_4)_2$ is an insulator. Consequently, the electronic entropy changes are negligible and can be disregarded. Similarly, the magnetic entropy changes in $Pb_3(VO_4)_2$ can be ignored either because the magnetic moments are absent. As mentioned above, $Pb_3(VO_4)_2$ undergoes a first-order ferroelastic phase transition at 357 K, and also exhibits a first-order ferroelectric phase transition at room temperature of 273 K. However, the entropy change associated with this ferroelectric phase transition is as small as 3.8 $J{\cdot}kg^{-1}{\cdot}K^{-1}$.[32,36] This can be attributed to the fact that $Pb_3(VO_4)_2$ undergoes changes primarily in the spontaneous polarization order parameter across the ferroelectric phase transition, while maintaining a consistent monoclinic crystal structure without significant alterations, leading to a relatively small lattice entropy change. In contrast, the ferroelastic phase transition in $Pb_3(VO_4)_2$ involves a structural transition from trigonal structure to monoclinic structure, accompanied by a significant volume contraction of -1.5%, resulting in a comparatively large entropy change. Therefore, the barocaloric entropy change induced by hydrostatic pressure in $Pb_3(VO_4)_2$ primarily arises from the lattice entropy associated with the first-order ferroelastic structural phase transition.

4. Conclusion and perspectives

In summary, we have investigated the BCE performance of $Pb_3(VO_4)_2$. This material undergoes a ferroelastic transition from a high-temperature trigonal structure to a low-temperature monoclinic structure at 357 K. It possesses high sensitivity to pressure with a pressure coefficient reaching up to 120 K/GPa in both heating and cooling cycles. Under a relatively low pressure of 80 MPa, $Pb_3(VO_4)_2$ shows significant pressure-induced isothermal entropy change of $\Delta S_{BCE} = 14\ J{\cdot}kg^{-1}{\cdot}K^{-1}$. We suggest the ferroelastic phase transition oxide as a novel category of BCE materials, showing promising potential for BCE refrigeration applications.

Acknowledgement

Project supported by the National Natural Science Foundation of China (Grant Nos. 52301241 and 52271175).

References

[1] Franco V, Blázquez J, Ipus J, Law J, Moreno-Ramírez L and Conde A 2018 *Prog. Mater. Sci.* **93** 112
[2] Gschneidner K A, Pecharsky V K and Tsokol A O 2005 *Rep. Prog. Phys.* **68** 1479
[3] Kumar A, Thakre A, Jeong D Y and Ryu J 2019 *J. Mater. Chem. C* **7** 6836
[4] Shi J, Han D, Li Z, Yang L, Lu S G, Zhong Z, Chen J, Zhang Q and Qian X 2019 *Joule* **3** 1200
[5] Chen J, Lei L and Fang G 2021 *Mater. Today Commun.* **28** 102706
[6] Imran M and Zhang X 2020 *Mater. Design* **195** 109030
[7] Cirillo L, Greco A and Masselli C 2022 *Therm. Sci. Eng. Prog.* **33** 101380
[8] Mañosa L and Planes A 2017 *Adv. Mater.* **29** 1603607
[9] Mañosa L, González A D, Planes A, Bonnot E, Barrio M, Tamarit J L, Aksoy S and Acet M 2010 *Nat. Mater.* **9** 478
[10] Mañosa L, González A D, Planes A, Barrio M, Tamarit J L, Titov I S, Acet M, Bhattacharyya A and Majumdar S 2011 *Nat. Commun.* **2** 595
[11] Yuce S, Barrio M, Emre B, Stern-Taulats E, Planes A, Tamarit J L, Mudryk Y, Jr. K A G, Pecharsky V K and Mañosa L 2012 *Appl. Phys. Lett.* **101** 071906
[12] Wu R R, Bao L F, Hu F X, Wu H, Huang Q Z, Wang J, Dong X L, Li G N, Sun J R, Shen F R, Zhao T Y, Zheng X Q, Wang L C, Liu Y, Zuo W L, Zhao Y Y, Zhang M, Wang X C, Jin C Q, Rao G H, Han X F and Shen B G 2015 *Sci. Rep.* **5** 18027
[13] Bermúdez-García J M, Sánchez-Andújar M, Castro-García S, López-Beceiro J, Artiaga R and Señarís-Rodríguez M A 2017 *Nat. Commun.* **8** 15715
[14] Bermúdez-García J M, Yáñez-Vilar S, García-Fernández A, Sánchez-Andújar M, Castro-García S, López-Beceiro J, Artiaga R, Dilshad M, Moya X and Señarís-Rodríguez M A 2018 *J. Mater. Chem. C* **6** 9867
[15] Lloveras P, Stern-Taulats E, Barrio M, Tamarit J L, Crossley S, Li W, Pomjakushin V, Planes A, Mañosa L, Mathur N D and Moya X 2015 *Nat. Commun.* **6** 8801
[16] Gorev M V, Mikhaleva E A, Flerov I N and Bogdanov E V 2019 *J. Alloys Compd.* **806** 1047
[17] Aznar A, Lloveras P, Romanini M, Barrio M, Tamarit J L, Cazorla C, Errandonea D, Mathur N D, Planes A, Moya X and Mañosa L 2017 *Nat. Commun.* **8** 1851
[18] Sagotra A K, Chu D and Cazorla C 2018 *Nat. Commun.* **9** 3337
[19] Flerov I N, Kartashev A V, Gorev M V, Bogdanov E V, Mel'nikova S V, Molokeev M S, Pogoreltsev E I and Laptash N M 2016 *J. Fluorine Chem.* **183** 1
[20] Kartashev A V, Gorev M V, Bogdanov E V, Flerov I N and Laptash N M 2016 *J. Solid State Chem.* **237** 269
[21] Gorev M V, Bogdanov E V and Flerov I N 2017 *Scr. Mater.* **139** 53
[22] Boldrin D, Mendive-Tapia E, Zemen J, Staunton J B, Hansen T, Aznar A, Tamarit J L, Barrio M, Lloveras P, Kim J, Moya X and Cohen L F 2018 *Phys. Rev. X* **8** 041035
[23] Matsunami D, Fujita A, Takenaka K and Kano M 2015 *Nat. Mater.* **14** 73
[24] Li B, Kawakita Y, Ohira-Kawamura S, Sugahara T, Wang H, Wang J, Chen Y, Kawaguchi S I, Kawaguchi S and Ohara K 2019 *Nature* **567** 506
[25] Lloveras P, Aznar A, Barrio M, Negrier P, Popescu C, Planes A, Mañosa L, Stern-Taulats E, Avramenko A, Mathur N D, Moya X and Tamarit J L 2019 *Nat. Commun.* **10** 1803
[26] He X, Kang Y, Wei S, Zhang Y, Cao Y, Xu K, Li Z, Jing C and Li Z 2018 *J. Alloys Compd.* **741** 821
[27] Ren Q, Qi J, Yu D, Zhang Z, Song R, Song W, Yuan B, Wang T, Ren W, Zhang Z, Tong X and Li B 2022 *Nat. Commun.* **13** 2293
[28] Zhang Z, Jiang X, Hattori T, Xu X, Li M, Yu C, Zhang Z, Yu D, Mole R, Yano S, Chen J, He L, Wang C W, Wang H, Li B and Zhang Z 2023 *Mater. Horiz.* **10** 977
[29] Mandal S and Ghosh A 1993 *Phys. Rev. B* **48** 9388
[30] Mandal S and Ghosh A 1994 *Phys. Rev. B* **49** 3131
[31] Hirofumi K, Talashi U and Hikaru T 1992 *J. Phys. Soc. Jpn.* **61** 2309
[32] Michio M, Hidetoshi K and Yoshihiro I 1981 *J. Phys. Soc. Jpn.* **50** 1592
[33] Hirofumi K, Talashi U, Hikaru T and Yoshihiro I 1991 *J. Phys. Soc. Jpn.* **60** 1169
[34] Hafner J and Kresse G 1997 *Properties of Complex Inorganic Solids*
[35] Perdew J P, Chevary J, Vosko S, Jackson K A, Pederson M R, Singh D and Fiolhais C 1993 *Phys. Rev. B* **48** 4978
[36] Denisova L T, Izotov A D, Irtyugo L A, Kargin Y F, Denisov V M and Beletskii V V 2016 *Dokl. Phys. Chem.* **466** 4